Journal of Applied Research and Technology

www.jart.icat.unam.mx

ICAT Instituto de Ciencias Aplicadas y Tecnología

Journal of Applied Research and Technology 24 (2026) 423-432

Original

Fusion Boundary Region in Single and Multi-Pass Dissimilar Metal Welds

Ivan Mendoza-Bravo*[1] • Doris Ivette Villalobos-Vera[1] and Miguel Ángel Cervantes-Moya[1]

[1]Tecnológico Nacional de México/Instituto Tecnológico de Veracruz, Departamento de Metal-Mecánica, Veracruz, Veracruz, Mexico.

Received: 27 06 2024; Accepted: 27 04 2025
Available: 30 04 2026

Abstract: Dissimilar metal welds between 2507 superduplex stainless steel and API X-52 carbon steel were joined using ER2594 via the gas metal arc welding process. Two joints were configured to be completed by single- and multipass welds to observe the effects of heat input and dilution on solidification across the fusion boundary region. Therefore, a dual etching technique was employed to reveal the microstructure across the interphase between the materials.

The optical microscopy analysis shows the microstructural evolution of the weld metal from blocky austenite to Widmanstätten, as dilution promotes redistribution of elements across the fusion boundary region, as observed in the EDS analysis. However, the WRC-1992 diagram indicates that this occurs at dilutions above ~36%. On the other hand, the weld metal/API X-52 interphase comprises an unmixed zone that exhibits morphologies such as beach, bay, and island and is a function of the percentage of base metal in the weld metal, with rapid cooling due to the weld metal's lower liquidus temperature. The tensile strength of both dissimilar welds is approximately equal and higher than that of the base metal, API X-52. The hardness distribution shows higher values in the weld metal/2507 of the multipass welding, reflecting the effect of heat input; however, it does not influence failure during the tensile test. This work analyzed and described the fusion boundary region in dissimilar welds for different joint designs and welding parameters.

Keywords: **Dissimilar metal weld, fusion boundary region, unmixed zone, dilution, solidification behavior.**

*Corresponding author.
E-mail address: ivan.mb@veracruz.tecnm.mx (Ivan Mendoza-Bravo).
Peer Review under the responsibility of Universidad Nacional Autónoma de México.

1. Introduction

Engineering must provide an energy supply at reasonable prices for an increasing world population. Oil, gas, and coal provide ~79% of global energy. In the Gulf of Mexico, production from mature fields is falling by 20% per year, forcing operators to drill ever deeper and explore more complex reservoirs. Operations are expected to experience pressure above 137 MPa (~20,000 Psi) and temperatures above 200 °C. Besides, high levels of hydrogen sulfide (H_2S) and carbon dioxide (CO_2) will drive the use of corrosion-resistant alloys (CRAs) (DNV, 2020). Therefore, the design of components under different operating conditions must consider the appropriate material for these components. 2507 Super-Duplex Stainless Steel (2507 SDSS) is used in subsea umbilicals as a connection between the platform's control station and the wellheads in water depths (Chai & Kangas, 2016). On the other hand, the API-52 carbon steel is widely used to transport crude from the offshore/onshore extraction points. Therefore, dissimilar metal welds (DMW) are necessary to link pipelines of both materials to provide a cost-effective solution.

Historically, dissimilar metal welds have been used in power generation. However, some failure incidents reported, have motivated researchers to study and understand the phenomena (Lundin, 1982; Siefert et al., 2011). The problem of DMW narrows down to the fusion boundary region (FBR) at the unmixed zone (UZ), localized at the internal limit of the weld metal/partial melted zone, which corresponds to a portion of the base metal melted and solidified without undergoing filler metal dilution (Savage et al., 1976a; Savage et al., 1976b; Baeslack et al., 1979; Nelson et al., 2000; Alexandrov et al., 2013). The differences in chemical composition, solidification temperatures and phases avoid epitaxial growth from base/weld metal. Instead, a white band or featureless zone is presented as an interphase. Doody (1992) resumes the morphologies of the unmixed zone as a function of their shape and appearance: beach, bay, and island. It has been identified that the UZ exhibits a compositional gradient associated with the segregation of alloying elements (Soysal et al., 2016; Knorr & McBee, 2009). This phenomenon has been studied by Kou (2012) and by Yang and Kou (2007a, 2007b), who evaluated the effects of the liquidus temperatures of the weld (TLW) and base metal (TLM) and proposed two macrosegregation mechanisms that explain the morphologies in the unmixed zone. Zhang et al. (2021) evaluated the fusion boundary region when $T_{LB}>T_{LW}$, and the welding process determines the peninsula morphology. The dilution has been related to the fusion boundary morphology, and redistribution of the elements occurs from the partial melting zone through the weld metal (Hytönen, 2023).

In the present work, the solidification in the fusion boundary region with different dilution rates was analyzed. The etching technique was crucial for observing the details, since a lack of detail can lead to misinterpretation. The etching technique allowed identifying the change in the initial solidification as ferrite to ferrite + austenite in the FBR, as the WRC-1992 diagram determined analytically. The findings can serve as a reference for establishing the welding parameters and dilution range when designing a dissimilar welding joint.

2. Materials and Methods

API X-52 carbon steel and 2507 superduplex stainless steel, both in pipe form with 10 cm (4 in) outer diameter and 0.06 cm (0.25 in) thickness, were used to fabricate weld coupons using ER 2594 superduplex stainless steel as the filler metal. The chemical compositions of the three alloys were determined by optical emission spectroscopy, as shown in Table 1.

To obtain different dilution rates, the joints were designed as a single V with 30 ° and 45 ° groove angles. The welding parameters are presented in Table 2 according to the manufacturer's recommendations, which is to keep the heat input range between 0.2 and -1.5 KJ/mm and interpass temperature below 150 °C (Sandvik, 1997).

The welds were performed using a rotary welding mechanism, with the GMAW torch positioned perpendicular. Thereafter, the welding coupons were sectioned using a band-saw cutting machine with water-based coolant,

Table 1. Chemical composition (wt %).

Alloy	Cr	Ni	Mo	Mn	Si	C	N	Fe	Cu	W	V	Nb
API X-52	0.043	0.065	0.021	1	0.241	0.201	-	98.09	0.149	0.004	0.061	0.015
2507 SDSS	25.86	7.4	4.272	0.420	0.353	0.019	0.3	63.12	0.117	0.030	0.056	0.008
ER 2594	21.72	7.32	3	0.509	0.490	0.060	0.20	66.17	0.267	0.038	0.198	0.019

in accordance with ASME IX, to obtain mechanical test samples and metallographic samples from the reduced section. Tensile tests were performed with a constant displacement rate of 0.2 mm/min.

The Vickers hardness test was performed using a 300 g load on the weld cross-section. Samples for metallographic observation with optical microscopy were prepared by grinding with SiC sandpaper and polishing with 6-, 3-, and 1-micron diamond paste. To reveal the microstructure with emphasis on the fusion boundary region, a double-step etching was performed using Nital reagent to stain carbon steel and the NaOH electroetching process to reveal the unmixed zone and the superduplex stainless steel.

Scanning electron microscopy observations and energy-dispersive X-ray spectroscopy (EDS) were performed to analyze elemental distributions around the fusion boundary in a single weld and to compare them with those in multipass welds affected by the heat input of subsequent passes.

Table 2. Welding parameters.

Variable	DMW-30	DMW-45
Groove angle (degree)	30	45
Root opening (mm)	0	1.6 mm
Welding passes	1 (Single)	3 (Multipass)
Welding Process	GMAW	
Welding Position	1G	
Polarity	CDEP	
Voltage (V)	22	
Amperage (A)	210	
Welding Speed (mm/s)	3.7	5
Interpass Temperature (°C)	-	150
Shielding gas	Argon 99%	

The dilution was determined through macrographs of the welds cross section, where the areas were colored to indicate the base and weld metal as shown in Figure 1. The measurement was performed using image analysis software. Dilution was calculated by dividing the area of the base metal within the weld metal by the total weld area.

To evaluate the effects of welding passes and dilution on the Ultimate Tensile Strength (UTS), samples were prepared in accordance with ASTM E8 for subsize specimens (W = 6 mm). The hardness mapping was performed in the cross-section of the DMWs.

3. Results and Discussion

3.1 Dilution Analysis

Figure 1A shows the macrograph of the DMW-30 with a single pass. The blue area (A_b = 25.21 mm^2) marks the joint preparation and the area to be completed by the ER 2594 filler metal. The red area (A_r = 2.59 mm^2) indicates the portion of the API X-52 inside the weld metal, whereas the 2507 SDSS is indicated by the yellow area (A_y = 3.81 mm^2).

Dilution in DMW-30 is given by:

$$\text{Dilution} = \frac{A_r + A_y}{A_r + A_y + A_b} \quad (1)$$

Then:

$$D_{DMW} = \frac{2.59+3.81}{2.59+3.81+25.21} = 0.202 = 20.2\% \quad (2)$$

The dilution in the dissimilar weld was calculated to be ~20%. However, to study the fusion boundary region between the API X-52/weld metal, the dilution was calculated independently.

The dilution was calculated independently, considering half of the area of the weld metal as follows:

$$D_{API} = \frac{2.59}{2.59+12.6} = 0.17 = 17\% \quad (3)$$

$$D_{2507SDSS} = \frac{3.81}{3.81+12.6} = 0.232 = 23\% \quad (4)$$

Hence, the dilution of the API X-52 into the weld metal represents 17%. The fusion line runs parallel to the bevel of the joint preparation. The average distance where the base metal comprises into base metal is ~0.36 mm.

On the other hand, the dilution with the 2507 SDSS is ~23%. The average distance of the fusion line into the base metal is ~0.6 mm. Table 3 summarizes the measurements from the DMW-45 in Figure 1B. The data was used to calculate the dilution for each welding pass. The dilution in the root pass was calculated considering both materials and thereafter each one independently.

Root pass considering both base metals:

$$D_{pass1} = \frac{4.38+1.97}{4.38+1.97+10.03} = 0.387 = 38.7\% \quad (5)$$

To evaluate the percentage of each base metal into weld metal, the equation was written as follows:

$$D_{pass1a} = \frac{4.38}{4.38+\left(\frac{10.03}{2}\right)} = 0.46 = 46\% \quad (5a)$$

$$D_{pass1s} = \frac{1.97}{1.97+\left(\frac{10.03}{2}\right)} = 0.28 = 28\% \quad (5b)$$

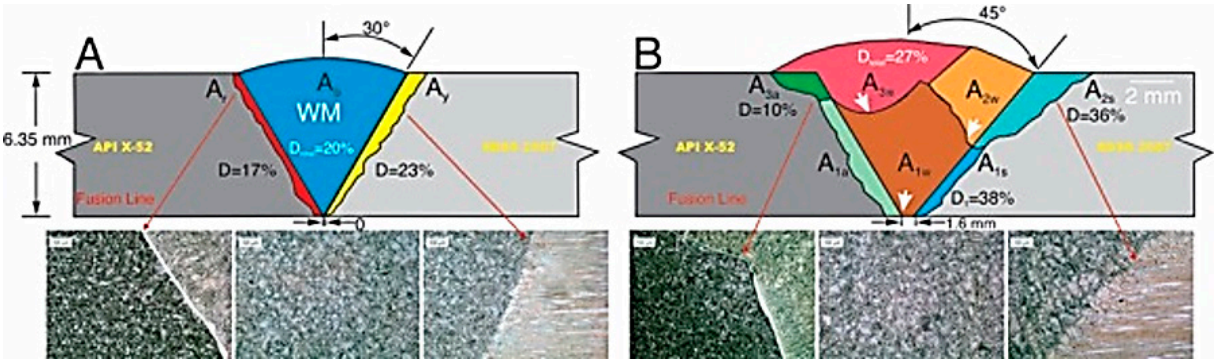

Figure 1. A) DMW-30 single-pass welding, B) DMW-45 multipass welding.

Then for the second pass that comprises the 2507 SDSS:

$$D_{pass2507SDSS} = \frac{6.09}{6.09+10.68} = 0.363 = 36.3\% \quad (6)$$

For the third pass related to the steel it is described as:

$$D_{API} = \frac{1.91}{1.91+16.67} = 0.102 = 10.2\% \quad (7)$$

The mean dilution of the DMW is considered as:

$$D_{total} = \frac{4.38+1.97+6.09+1.91}{4.38+1.97+6.09+1.91+10.03+10.68+16.67} = \frac{14.35}{51.73} = 27.7\% \quad (8)$$

The mean dilution of the DMW-45 is estimated around 27%. Nevertheless, the dilution analysis allows us to determine that the root pass in the side of the API steel experienced the higher dilution (D=46%). However, the lowest dilution is presented in the same base metal at the third pass (D=10%). Those results indicated that the microstructure in the FBR will be different.

The study of the dilution effect on the final microstructure was performed with the WRC-1992 diagram (Kotecki & Siewert, 1992). The Chromium equivalent (Cr_{eq}) and Nickel equivalent (Ni_{eq}) in Table 4 were calculated using Equations 9 and 10 and the chemical composition in Table 1.

$$Cr_{eq} = \%Cr + \%Mo + (0.7 \times \%Nb) \quad (9)$$

$$Ni_{eq} = \%Ni + (35 \times \%C) + (20 \times \%N) + (0.25 \times \%Cu) \quad (10)$$

Figure 2 shows a portion of the WRC-1992 diagram used to analyze the dissimilar metal weld. Initially, a line was traced connecting the API-X52 and 2507 SDSS, and the midpoint is marked with a pink diamond, representing the synthetic mix of both base metals. Thereafter, the line from ER 2594 (red square) to the pink diamond represents the hypothetical mix of the weld metal. Considering the fractions of the line as a percentage of dilution, then the lowest dilution (10%) calculated in Eq. 7 is represented by a green circle located in the F field with a ferrite number (FN) of 21. On the other hand, the highest dilution (46%) is represented with a cyan circle, which is located into the FA field, with FN=9.

Table 3. Measurement of welding pass in DMW-45.

Welding Pass	1			2		3	
	A_{1a}	A_{1w}	A_{1s}	A_{2s}	A_{2w}	A_{3a}	A_{3w}
Area (mm^2)	4.38	10.03	1.97	6.09	10.68	1.91	16.67

It is important to consider that the transition from ferrite (F) to ferrite + austenite (FA) was calculated to be ~36% of dilution, identified with a yellow star.

Table 4. Values of Cr_{eq} and Ni_{eq}.

Material	Cr eq	Ni eq
API X-52	7.13	0.07
2507	30.13	14.09
ER 2594	24.73	13.48

3.2 Microstructural Analysis

The transition from API X-52 →weld metal shows a microstructural discontinuity at the fusion boundary region where epitaxial growth from the base to the weld metal does not occur. Instead of a white band, an interface forms, termed a “unmixed zone,” consisting of base metal that has been melted and solidified without mechanical mixing with the filler metal (Savage et al., 1976a).

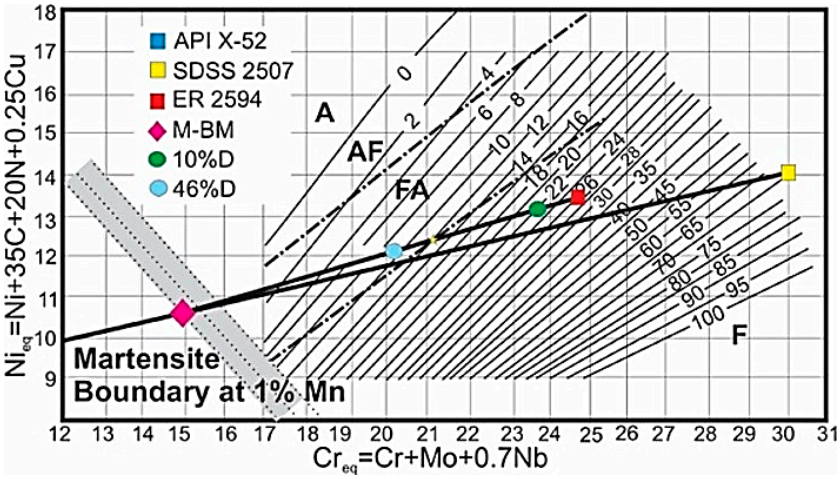

Figure 2. Dilution analysis of single and multi-pass DMWs using the WRC-1992 diagram.

In both welds DMW-30 and DMW-45, the unmixed zone is present with different thicknesses and morphologies.

The beach type in Figures 3B and 3E is common in both welds. The thickness measurements for single- and multi-pass welds are shown in Table 5 and are not wide enough to form a bay morphology.

The unmixed zone bay-type is formed in the root pass as shown in Figures 3C and 3F. This morphology can be distinguished from the beach because the bay-type is wider, its boundaries are not well-defined, and it has an irregular shape. Furthermore, it may be related to the high dilution calculated in Equation 5a.

Table 5. Thickness measurement in the beach morphology along the dissimilar metal welds.

Weld	Min (µm)	Max (µm)	Mean (µm)	Std Dev.
DMW-30	2.04	18.04	8.36	4.12
DMW-45	1.89	14.86	7.23	2.62

On the other hand, the cover pass shows the formation of the peninsula morphology, identifiable by the presence of weld metal surrounding the base metal as shown in Figures 3A and 3D.

The formation of the unmixed zone and their morphologies can be related to the difference in the chemical composition and liquidus temperature of the base and weld metal, which determine the segregation patterns in the fusion boundary region. In this dissimilar weld, the liquidus temperature of the API X-52 is T_{LB}=1498 °C and the weld metal T_{LW}=1402 °C. According to Kou (2012) (Soysal et al., 2016; Yang & Kou, 2007a; Yang & Kou, 2007b) the dissimilar weld follows the macrosegregation mechanism I, when $T_{LW}<T_{LB}$.

The microstructural evidence indicates that a portion of the partial melting zone (PMZ) becomes part of the unmixed zone if liquation occurs along the grains, and that differences in liquidus temperatures promote faster cooling to reach the weld metal temperature. It can be considered that the beach and bay morphologies of the unmixed zone depend on the width of the partially melted zone, which is the interface between the base/weld metal.

Zhang et al. (2021) suggested that the peninsula morphology is formed during the early stages of solidification and not during the liquid state. That is why the base metal into the weld metal maintains the bainite microstructure as shown in Figure 3A.

The morphologies of the SDSS weld metal shown in Figure 3 have been reported in duplex stainless steel weld metals with $Cr_{eq}/Ni_{eq} < 2.40$, which can solidify as primary ferrite (Widmanstätten) or a mix of ferrite and austenite (blocky) (Sharafi, 1993). According to the WRC-1992 analysis, at a dilution of around 36% and a Creq/Nieq ratio of 1.7, solidification will behave as follows: F ≤ 1.7; Cr/Ni ≥ F + A.

The blocky morphology seems to grow from the unmixed zone, working as a substrate. Considering that the weld metal can solidify as F+A, epitaxial growth is favored because the crystal lattices are similar and slight variations in chemical composition occur (Zhang et al., 2021). The redistribution of elements into the FBR is shown in Figure 4 and is promoted by elements that mix during the liquid state or by macrosegregation (Kou, 2012). In this

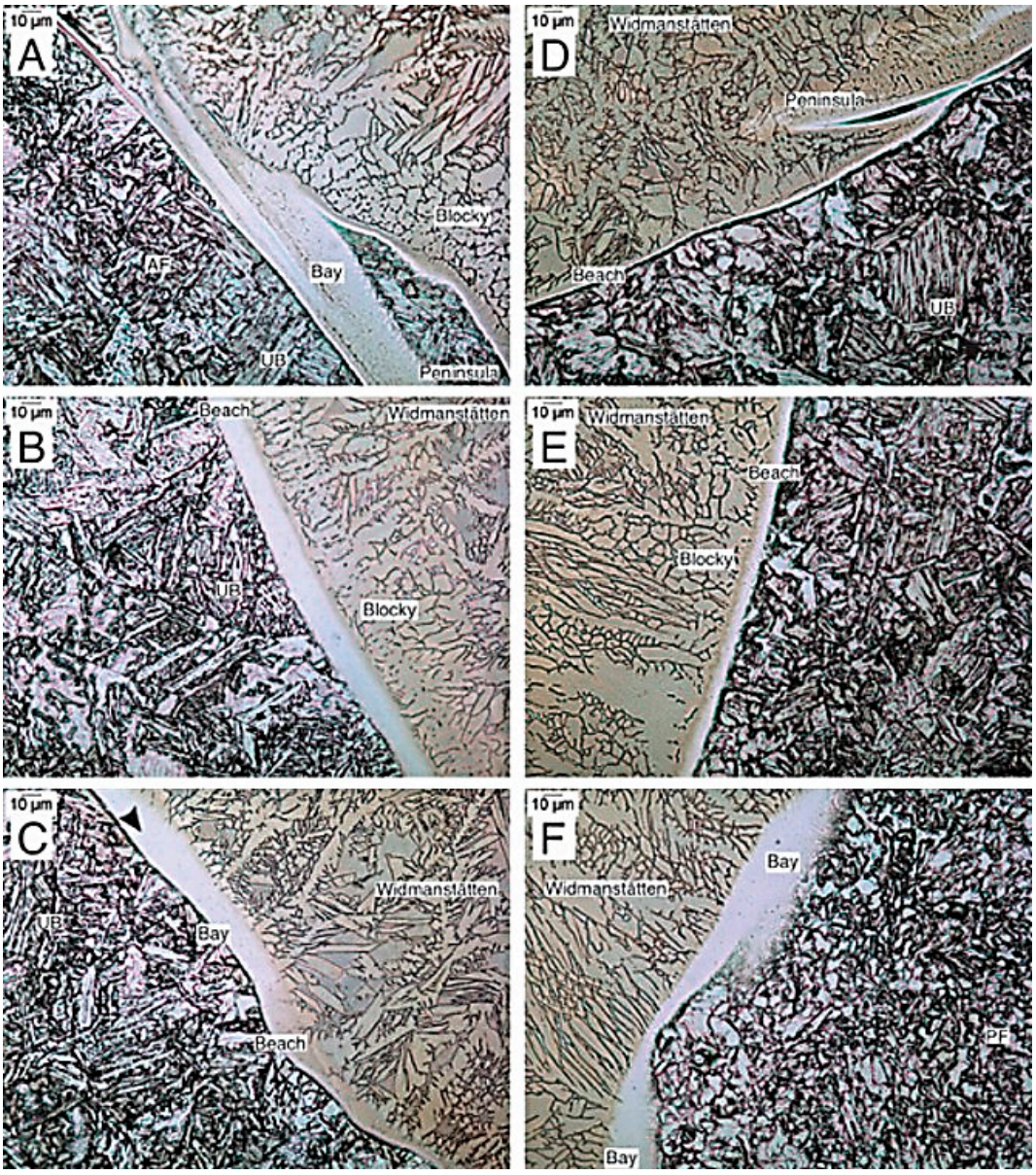

Figure 3. Fusion boundary region in single and multipass DMW.

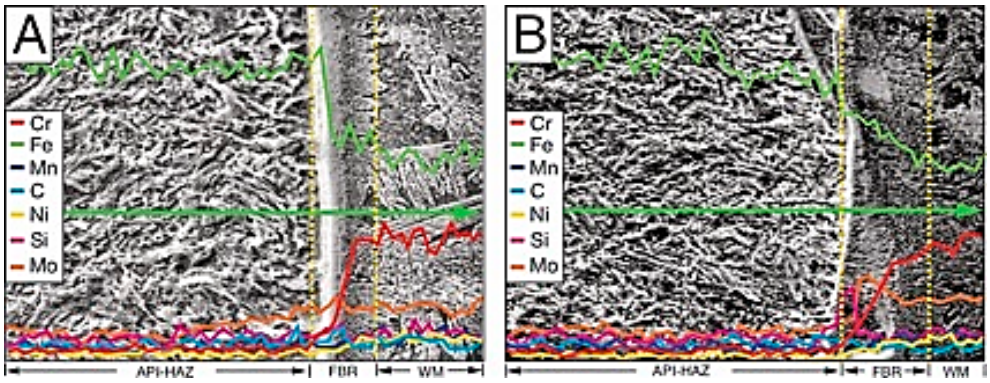

Figure 4. EDS Line scan of the distribution of elements through the fusion boundary region from the SDSS weld metal to API X-52.

case, macrosegregation is considered due to the slope in the EDS analysis in elements such as Fe, Cr, and Mo in both welds.

Beyond the FBR, weld metal shows an evolution from blocky to Widmanstätten morphology. The microstructural characterization allows us to observe the growth of the austenite from blocky as columnar dendritic oriented with the heat flow, which favors the chemical composition to be stabilized as a standard duplex alloy, as shown in Figure 4, hence Cr_{eq}/Ni_{eq} ratio will be below 1.7, resulting in the ferrite/austenite balance, as the microstructure shows in Figure 3 and the WRC-1992 predicted.

3.3 Mechanical Properties

The microhardness values from measurements along the cross-section of the DMW-30 and DMW-45 were averaged and colored around the indentation. At a glance, the hardness map in Figure 5A shows the single-pass weld. On the left side, the API X-52 exhibits an increase in hardness from 100 HV to 250 HV over ~3 mm. The blue/sky-blue area corresponds to the heat-affected zone, where upper bainite (UB) forms due to welding thermal cycles and is characterized as harder than ferrite.

The cyan line marks the fusion boundary region and serves as a transition from the blue to the green area, where weld metal forms in blocky morphology, which is in good agreement with the microstructural characterization in Figure 3A-C. The right side, a yellow-orange transition area corresponding to the SDSS 2507 HAZ, delimits the weld metal. The red area (~350HV) on the surface of the weld metal is due to the surface losing heat faster than the inner weld metal, promoting an incomplete eutectoid reaction (F→F+A), resulting in a higher percentage of ferrite and, hence, harder zones.

The hardness maps in Figure 5B illustrate the DMW-45 multipass weld. The left side shows the API X-52 steel, with the same hardness distribution pattern as the DMW-30 in Figure 5A. The difference is observed in the heat-affected zone adjacent to the first welding pass, which is wider than that adjacent to the third pass (top area) due to heat input from the second and third passes, even though the interpass temperature was below 150 °C. The hardness in the weld metal varies with each welding pass, and only the area near the fusion boundary region shows an average of ~250 HV (green area), attributed to the blocky morphology. The weld metal corresponding to the second pass shows a hardness of ~325 HV, similar to the SDSS 2507 HAZ and the base metal.

Figure 6 shows the stress-strain curve where the yield strength value for single pass (DMW-30) is around 420 MPa

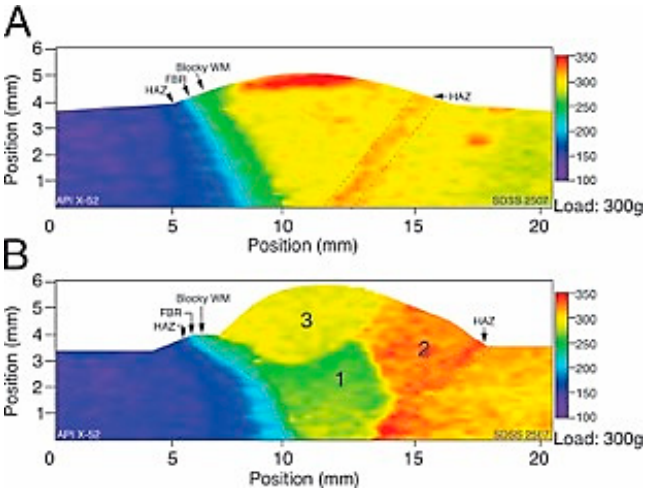

Figure 5. Hardness in the cross section of A) DMW-30 and B) DMW-45.

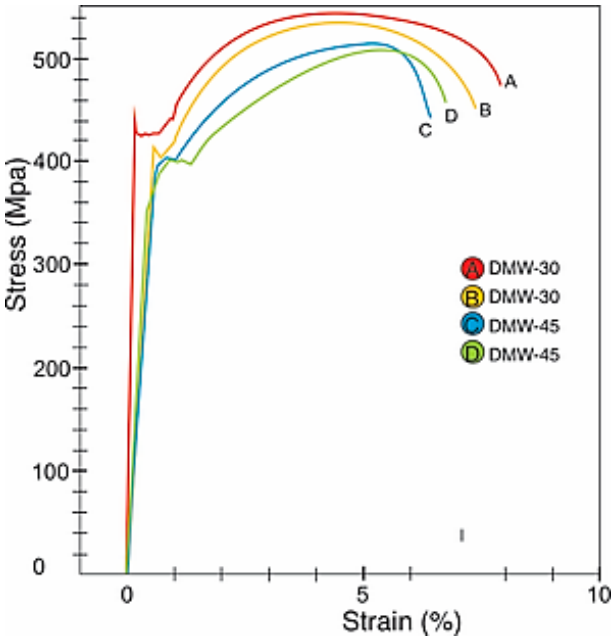

Figure 6. Stress-strain curve for single pass (DMW-30) and multi-pass (DMW-45).

and for multi-pass weld (DMW-45) is 400 MPa, where the Young´s modulus is 52 GPa. The ultimate tensile strength for single-pass welds is 540 MPa, whereas for multi-pass welds it is around 500 MPa.

Figure 7A-B shows the location of the fractures. In both cases, the fracture initiated in the API X-52 steel, not in the heat-affected zone. Besides, both DMWs show that the values were higher than 352 MPa (52000Psi) which is the nominal stress for the API X-52 steel.

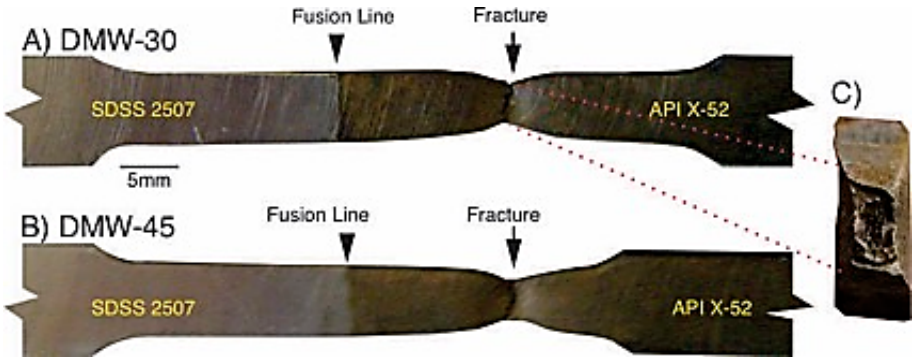

Figure 7. Fracture location in the DMWs.

The reduction in area (Z) during necking of the DMW-30 was calculated to be 71%. The value of Z for the DMW-45 was calculated at 68%. The representative fractography is shown in Figure 7C. Considering the strain percentage and Z values of both dissimilar metal welds, a ductile fracture can be considered.

The tensile test of the dissimilar metal welds showed that the fusion boundary region has no influence on the UTS; hence, it is difficult to measure the effect of metallurgical phenomena (morphologies, macrosegregation, etc.).

The design of the joint increases the size of the heat-affected zone, which may account for the difference in strain between single- and multipass DMW, but not for fracture initiation.

Conclusions

To analyze dissimilar metal welds, metallographic practice is fundamental, and the selection of etching reagents plays an important role in accurately revealing the features of the fusion boundary region. The WRC-1992 diagram estimates the transition from F to F+A as a function of the element distribution. The results highlight the effect of the dilution on the final microstructure, and the following conclusions can be drawn:

1. Weld dilution determined the width of the unmixed zone in the fusion boundary region and the morphology of the UZ, as shown in Figure 3. Beach and bay morphology are common for low dilution rates, but they are not continuous along the fusion line in a single welding pass.
2. Weld metal morphology evolves from blocky (F) to Widmanstätten (F+A) according to the WRC-1992 analysis at a dilution around 36% and Cr_{eq}/Ni_{eq} ratio of 1.7, where the solidification will behave as: $F \leq 1.7_{Cr/Ni} \geq F+A$.
3. At low dilution ≤ 36% the unmixed zone works as a substrate for the solidification of the weld metal since the crystalline lattice is the same.
4. Elements redistribution in the FBR can occur in liquid state during welding or during solidification via macrosegregation due to the differences in liquidus temperatures of the weld and base metal.
5. The ultimate tensile strength is not affected by the morphologies of the unmixed zone. Nevertheless, the hardness map shows that unmixed zone is harder than the base metal, which is the effect of the dilution between the base and filler metal.

Funding

This research was supported by Tecnológico Nacional de México “Proyectos de Investigación Científica, Desarrollo Tecnológico e Innovación, Grant No. 14501.22-P”.

Conflict of Interest

The authors declare that they have no conflicts of interest to disclose.

References

DNV. (2020) Technology uptake: Oil, Gas & Coal, *DNV Technology outlook 2020*. 44-48.
https://www.dnv.com/publications/new-directions-complex-choices-the-outlook-for-the-oil-and-gas-industry-in-2020-165515/

Alexandrov, B. T., Lippold, J. C., Sowards, J. W., Hope, A. T., & Saltzmann, D. R. (2013). Fusion boundary microstructure evolution associated with embrittlement of Ni–base alloy overlays applied to carbon steel. *Welding in the World*, *57*(1), 39-53.
https://doi.org/10.1007/s40194-012-0007-1

Baeslack III W.A., Lippold J.C. & Savage W.F. (1979) Unmixed Zone Formation in Austenitic Stainless-Steel Weldments, *Welding Journal 58* (6),168-s – 176-s.
https://aws-p-001-delivery.sitecorecontenthub.cloud/api/public/content/68c29818a7ac44b78946be1883bc34fc?v=fdff3e1b

Chail, G., & Kangas, P. (2016). Super and hyper duplex stainless steels: structures, properties and applications. *Procedia Structural Integrity*, *2*, 1755-1762.
https://doi.org/10.1016/j.prostr.2016.06.221.

Doody, T. (1992). Intermediate mixed zones in dissimilar metal welds for sour service. *Welding journal*, *71*(3), 55-60.
https://www.aws.org/Magazines-and-Media/Publication-Archive/?__hstc=24525925.5cf8b51cd577c68f4fd48cc4c47d0970.1699540175432.1709566018237.1709568073539.160&__hssc=24525925.1.1709568073539&__hsfp=1530836998#sort=%40publishedon%20descending&numberOfResults=5&f:@assettype=[Welding%20Journal]&f:@yearofpublication=[1992]&f:@publishedonmonth=[03]

Hytönen, N., Ge, Y., Que, Z., Lindqvist, S., Nevasmaa, P., Virkkunen, I., & Efsing, P. (2023). Study of fusion boundary microstructure and local mismatch of SA508/alloy 52 dissimilar metal weld with buttering. *Journal of Nuclear Materials*, *583*, 154558.
https://doi.org/10.1016/j.jnucmat.2023.154558

Knorr D.B. & McBee J.J. (2009) Near Weld Interface Compositional Variations in Low-Alloy Steel Weldments, *Welding Journal 88* (10) 202-s – 211-s.
https://aws-p-001-delivery.sitecorecontenthub.cloud/api/public/content/ae77fcd2da0547308885d1749923adcb?v=b46666a9

Kotecki, D. J., & Siewert, T. A. (1992). WRC-1992 constitution diagram for stainless steel weld metals: a modification of the WRC-1988 diagram. *Welding Journal*, *71*(5), 171-178.
https://aws-p-001-delivery.sitecorecontenthub.cloud/api/public/content/5ed8cac0fedc475eb45356947da65296?v=da20b9c4

Kou, S. (2012). Fluid flow and solidification in welding: Three decades of fundamental research at the University of Wisconsin. *Weld. J*, *91*(11), s287-s302.
https://aws-p-001-delivery.sitecorecontenthub.cloud/api/public/content/5684ff83ac2e4744bc0fe2aed4abb5f2?v=4e7ccf18

Lundin C.D. (1982) Dissimilar Metal Welds – Transition Joints Literature Review, *Welding Journal 61* (2), 58-s – 62-s.
https://aws-p-001-delivery.sitecorecontenthub.cloud/api/public/content/7d2ce6ac004e428382f302fcbc5c4ee4?v=aca9b392

Nelson, T. W., Lippold, J. C., & Mills, M. J. (2000). Nature and evolution of the fusion boundary in ferritic-austenitic dissimilar metal welds—part 2: on-cooling transformations. *Welding Research*, *10*, 267-277.
https://aws-p-001-delivery.sitecorecontenthub.cloud/api/public/content/d4cbb0b79fbf4e398d6d0bd1cceff4de?v=5dc0b9d9

SANDVIK (1997) S-187-ENG, Sandvik SAF 2507 A high performance duplex stainless steel UNS S32750, Sandvik Steel, Sandviken, Sweden.
Savage, W. F., EF, N., & TW, M. (1976b). Microsegregation in 70Cu-30Ni weld metal.
https://aws-p-001-delivery.sitecorecontenthub.cloud/api/public/content/da0ea2ec23d543aa8a8d6b12f907d0e7?v=c7ff3e50

Savage, W. F., Nippes, E. F., & Szekeres, E. S. (1976a). Study of weld interface phenomena in a low alloy steel. *Welding Journal*, *55*(9), 260.
https://aws-p-001-delivery.sitecorecontenthub.cloud/api/public/content/9c0b8e7f494b46a8a0ef7786381334b0?v=931d6cab

Sharafi, S. (1993). *Microstructure of super-duplex stainless steels* (Doctoral dissertation, University of Cambridge).
https://www.phase-trans.msm.cam.ac.uk/2007/Sharafi/Pt1.pdf

Siefert J.A., Tanzonsh J. M., Shingledecker J.P., & Newll Jr. W.F., (2011) EPRI P87: A promising New Filler Metal for Dissimilar Metal Welding, *Welding Journal 90* (3), 30 – 34.
https://www.aws.org/Magazines-and-Media/Publication-Archive/?__hstc=24525925.5cf8b51cd577c68f4fd48cc4c47d0970.1699540175432.1709566018237.1709568073539.160&__hssc=24525925.1.1709568073539&__hsfp=1530836998#sort=%40publishedon%20descending&numberOfResults=5&f:@assettype=[Welding%20Journal]&f:@yearofpublication=[2011]&f:@publishedonmonth=[03]

Soysal, T., Kou, S., Tat, D., & Pasang, T. (2016). Macrosegregation in dissimilar-metal fusion welding. *Acta Materialia*, *110*, 149-160. https://doi.org/10.1016/j.actamat.2016.03.004

Yang, Y. K., & Kou, S. (2007a). Fusion-boundary macrosegregation in dissimilar-filler metal Al-Cu welds. *WELDING JOURNAL-NEW YORK-*, *86*(11), 331. https://aws-p-001-delivery.sitecorecontenthub.cloud/api/public/content/e1e84ddcc64c4ca78bdf802c4780dfa7?v=23fc3393

Yang, Y. K., & Kou, S. (2007b). Weld-bottom macrosegregation caused by dissimilar filler metals. *WELDING JOURNAL-NEW YORK-*, *86*(12), 379. https://aws-p-001-delivery.sitecorecontenthub.cloud/api/public/content/49be7f83e9674ccdaa51a2df87d64633?v=402a7c94

Zhang, Y., Cai, Z., Li, X., Huo, X., Fan, M., Li, K., & Pan, J. (2021). Investigation on solidification and phase transformation of heterogenous interface structure in dissimilar metal weld between high Cr heat-resistant steel and nickel-based alloy 617. *Journal of Manufacturing Processes*, *62*, 257-261. https://doi.org/10.1016/j.jmapro.2020.11.039